

Stability and mode analysis of solar coronal loops using thermodynamic irreversible energy principles II.

Modes in twisted non–isothermal magnetic field configurations

A. Costa*

Instituto de Astronomía Teórica y Experimental (IATE–CONICET), Córdoba, Argentina

R. González

*Universidad Nacional de General Sarmiento (UNGS), Argentina,
Departamento de Física (FCEyN-UBA) Buenos Aires, Argentina*

(Dated:)

Abstract

We study the stability and the modes of non – isothermal coronal loop models with different intensity values of the equilibrium twisted magnetic field. We use an energy principle obtained via non – equilibrium thermodynamic arguments. The principle is expressed in terms of Hermitian operators and allows to consider together the coupled system of equations: the balance of energy equation and the equation of motion, to obtain modes and eigenmodes in a spectrum ranging from short to long–wavelength disturbances without having to use weak varying approximations of the equilibrium parameters. Long–wavelength perturbations introduce additional difficulties because the inhomogeneous nature of the medium determines disturbances leading to continuous intervals of eigenfrequencies which cannot be considered as purely sinusoidal. We analyze the modification of periods, modes structure and stability when the helicity, the magnetic field strength and the radius of the fluxtube are varied. The efficiency of the damping due to the resonant absorption mechanism is analyzed in a context of modes that can either impulsively release or storage magnetic energy. We find that the onset of the instability is associated to a critical value of the helicity and that the magnetic energy content has a determinant role on the instability of the system with respect to the stabilizing effect of the resonant absorption mechanism.

*Electronic address: A. Costa: acosta@mail.oac.uncor.edu

I. INTRODUCTION

A. Variational principle

A crucial requirement for any theoretical model of coronal structures is to give account of the stability and evolution of far-from-equilibrium states which are responsible of the characteristic rich topology and dynamics of the solar corona. This implies to consider the coupling of thermal and mechanical equations. Different stability analysis of solar structures can be found in the literature, generally restricted to special types of perturbations and specific equilibrium models. These includes, models that consider adiabatic configuration such as the ones analyzed via the classical criterion of Bernstein [4] or those that presuppose static equilibrium and analyze thermal stability. In the application of Bernstein's criterion, the adiabatic assumption implies that the energy balance equation is not required and thus dissipation is impossible. Also the assumption of static models is a strong, and often unjustified, restriction for open systems.

In this paper we apply an energy principle to analyze the stability of solar coronal loops when helical modes are present. The principle was obtained in previous papers (Paper I: [5]; [6]; see also [20]) using a general procedure of irreversible thermodynamics -based on firmly established thermodynamic laws- that can be understood as an extension of Bernstein's MHD principle to situations far from thermodynamic equilibrium.

In Paper I and in [6] we showed how to obtain the variational principle for solar coronal structures from the equations that describe the dynamics of the system. The method consists of obtaining a Lyapunov function, also known as generalized potential, that represents the mathematical expression of the stability conditions. The principle is subject to physically reasonable requirements of hermiticity and antihermiticity over the matrices. For a more detailed presentation see Paper I and the references therein.

B. Solar coronal loops

MHD loop oscillations in the corona are known to be strongly damped, mostly having decaying times of few periods $N_p \approx 2 - 7$ periods. While thermal conduction, with the contribution of radiative cooling mechanisms, could be the main cause of the damping of pure MHD slow magnetoacoustic mode oscillations they are unimportant for the MHD fast

modes. Resonant absorption and phase mixing seem more promising in giving account of the rapid decay ([11]; hereafter HG, [10]) of the ideal fast oscillations of these strongly inhomogeneous and structured plasma systems. Inhomogeneous equilibrium distributions of plasma density and temperature varying continuously across the magnetic field led to plasma waves with continuous intervals of eigenfrequencies. The occurrence of the Alfvén ideal MHD continuum in a thin edge layer is derived from the highly anisotropic character of the fast magnetoacoustic waves giving rise to a peak of the amplitudes where the perturbation develops large gradients and the absorption has maxims. However, there is another type of continuum commonly known as slow magnetosonic continuum associated to the inhomogeneity of the equilibrium parameters along the axis of the loop (see Paper I). This inhomogeneities are associated, for example, to changes in the density concentration at the loop basis. If the magnetic field is twisted the inhomogeneities led to the coupling of Alfvén and slow magnetosonic continuum modes ([3]).

The resonant absorption mechanism of wave heating consists on the non-dissipative transference of wave energy from the collective line-tied wave with fast discrete eigenvalues (kinetic energy of the fast radial component) to a local resonant mode in the Alfvén continuum, (kinetic energy of the azimuthal component), which is then dissipated in an enhanced manner. Then, the continuum oscillations are converted into heat by dissipative processes; as the medium has large gradients in the Alfvén speed, the oscillations of neighboring field lines become out of phase and shear Alfvén waves lead to enhanced viscous and ohmic dissipation (see [12] for the linear regime and [14] for the nonlinear one). The mode conversion from the collective to the local mode occurs in a time that is non-dissipative and generally much shorter than the second time scale which is related to the dissipative damping of the small-scale perturbations of the local mode in the resonance layer ([18]; [22]).

The whole temporal pattern description of modes that exhibit a combination of global (discrete line-tied fast eigenmode) and localize (Alfvén continuum mode) behaviour is known as quasi-mode. Moreover, the mixed nature of the modes is not only due to the temporal behaviour but also to the boundary value problem giving rise to a spatial behaviour which is also of a mixed nature, i.e. coronal loops with line-tying constraints cannot support pure waves: Alfvén, slow or fast magnetoacoustic modes. HG studied the mixed spectral description of coronal loops (i.e. the resulting superposition of basic waves which adjust the line-tied condition) without assuming a straight magnetic field and forcing the loop

to follow the photospheric velocity perturbations. They found that pure Alfvén and pure slow modes are obtained as singular limiting cases of cluster spectra of Alfvén–fast or slow–fast modes, where the fast components are localized in a photospheric boundary associated to the line–tied condition: the coronal part of the loop acting as a resonant cavity of large Alfvén components and fast components, with a small but rapidly varying amplitude, located in the photospheric boundary layer. They found that heating of coronal loops by resonant absorption is due to the line–tied Alfvén continuum which no longer depends on the poloidal magnetic field and that the corresponding eigenmodes have a global ballooning feature which is characterized by an accumulation point given by the Alfvén frequency. In [9] (hereafter GH), a variational principle, based in Bernstein’s principle, was obtained to derive the Alfvén and slow continuum frequencies in a line–tied inhomogeneous cylinder. Stability considerations led them to conclude the global stability of coronal loops.

In this paper, following results of Paper I we apply our energy principle to consider the stability and mode structure of loop inhomogeneous coronal models with non–vanishing helicity. Our principle has the advantages that it does not require a WKB approximation and that, as was mentioned, it allows the consideration of the coupling of the thermal and mechanical equations that are necessary to analyze far from equilibrium states.

II. THE MHD STABILITY CRITERION FOR CORONAL STRUCTURES

Solar coronal conditions with large Reynolds numbers are well fitted by ideal MHD plasma models (i.e. infinite electrical conductivity $\sigma \gg 1$ leading to vanishing viscosity and ohmic dissipation). Thus, the fundamental equations considered are the mass conservation equation, the perfect gas law or state equation for a fully ionized H plasma and the induction equation, with vanishing magnetic diffusivity due to the conductivity properties. The energy balance equation takes the form:

$$\frac{\rho^\gamma}{(\gamma - 1)} \frac{D}{Dt} \left(\frac{p}{\rho^\gamma} \right) = -\nabla \cdot \vec{F}_c - L_r + H \quad (1)$$

\vec{F}_c is the heat flux due to particle conduction along the loop, L_r is the net radiation flux and H the heating function which was chosen as in Paper I: $H = h\rho + H_0$. Eq. 1 expresses the fact that the gain in particle energy (internal plus kinetic) is due to the external heating sources represented by the heating function, heat flow and radiation losses; all other heating

sources were considered as vanishing terms implying that the optically thin assumption holds. Note that the non-ideal contribution in the energy equation (L) is associated to the open character of the loop system.

Once the linearization around a nonlinear equilibrium or stationary state is performed, and after a straightforward manipulation procedure where the hermiticity requirements are fulfilled the generalized energy principle and the respective frequencies are obtained (Paper I and [6]) as:

$$\delta^2 W_p = \frac{1}{2} \int (\vec{\xi}^* \beta F \vec{\xi} + T_1^* A T_1 + T_1^* B \vec{\xi} - \vec{\xi}^* B T_1) d^3 x \geq 0. \quad (2)$$

$$\omega^2 = - \frac{\int (\vec{\xi}^* \beta F \vec{\xi} + T_1^* A T_1 + T_1^* B \vec{\xi} - \vec{\xi}^* B T_1^*) d^3 x}{\int (\vec{\xi}^* \beta \rho_0 \vec{\xi}) d^3 x} \quad (3)$$

with the same normalization condition as in Paper I. F is the known Bernstein operator for the system, ξ and T_1 are the motion and temperature perturbations and operators A and B are as in Paper I. For the non-dissipative cases ($L = 0$ or equivalently $T_1 = 0$), last expressions (discarding the presence of factor β which appears in the equations to fit the Hermitian and anti-Hermitian conditions) are reduced to the well-known Bernstein MHD energy principle and its respective frequencies.

III. APPLICATION TO AN INHOMOGENEOUS LOOP MODEL WITH NON-VANISHING HELICITY

On one hand, the azimuthal component of the loop perturbation is believed to be one of the principle responsible of resonant absorption and damping of ideal oscillations; on the other, this component is associated to the storage of magnetic energy in systems with non-vanishing helicity which eventually is released by instabilities. Thus, we are interested in analyzing the changes produced in the stability of non-homogeneous loops subject to helical perturbations. This is, loops with inhomogeneous distributions of plasma density and temperatures subject to body modes and with non-vanishing helicity. In this case, the Alfvén, slow and fast magnetoacoustic cylinder modes cannot longer be associated to the azimuthal, longitudinal and radial components respectively. The observational importance of helical modes cannot be neglected and it is poorly known how helicity affects important physical features of mode oscillations (e.g., damping mechanisms, stability and periods). However, a mode classification can be accomplished via the analysis of the mode variations,

described in an orthogonal basis, while helicity is varied. The basis is formed by the orthogonal displacements: parallel and perpendicular to the magnetic field and the radial (and perpendicular to the surface of the tube) one, of observational interest.

The fundamental modes are generally observationally and energetically more important than their harmonics. For these global modes the inhomogeneous nature of the medium cannot be ignored and it determines the structure of the disturbance which cannot be taken as sinusoidal, making the traditional normal mode analysis useless for this treatment (sinusoidal dependence with constant coefficients), i.e. at least a WKB approximation, of weakly varying parameters compared to a typical wavelength, is required. Moreover, the occurrence of either an infinitely degenerate eigenvalue or an accumulation point giving rise to a continuous spectrum are associated to inhomogeneities. We consider two types of inhomogeneities: the inhomogeneity of the equilibrium parameters along the loop axis, and the inhomogeneity across the loop axis when the radius is varied. As a first order approximation we neglect the effect of gravitational stratification and thus confine the analysis to characteristic spatial scales lower than the pressure scale height in the solar corona. In order to analyze the stability and to obtain the frequencies and modes the physical quantities in eq. 2 and eq. 4 must be calculated along the loop structure.

A. Mechanical equilibrium

To determine an equilibrium configuration we assume force-free equations. This assumption is justified for coronal conditions due to the fact that in plasmas with low β (gas pressure over the magnetic pressure) the pressure gradient can be neglected in comparison to the Lorentz force. For the chromosphere and the photosphere the force-free approximation may not be a good one. However, it is a widespread supposition [19]: perturbed systems are believed to relax to new force-free, minimum energy states and chromospheric conditions seem to be well fitted to force-free models from $4 \cdot 10^5$ m [2] (Chapter 5).

Coronal loops are generally modeled as thin cylindrical fluxtubes where the curvature and related forces can be neglected so the cylindrical geometry can be applied. The fluxtube is assumed as line-tied to the photospheric plasma through its footpoints which are forced to follow the photospheric velocity perturbations. The random velocity field creates vorticity generally twisting the coronal fluxtubes. Thus, a relation between the helical twist and

the force-free parameter can be derived as follows (e.g. [21]). The coronal loop model is obtained from the equations

$$\nabla \times \mathbf{B}_0 = \alpha(r)\mathbf{B}_0 \quad \mathbf{j} \times \mathbf{B}_0 = 0. \quad (4)$$

Also, since \mathbf{B}_0 is force-free, $\nabla p = 0$ everywhere and thus has a constant value along the loop. We consider a straight cylinder with a nonuniform distribution of density and temperature and a resulting uniform twist over an initially non-rotated field $\mathbf{B} = (0, 0, B_z)$ yielding the unperturbed magnetic field

$$\mathbf{B}_0 = (B_r, B_\phi, B_z) = B_0(0, \frac{br}{\Delta}, \frac{1}{\Delta})$$

with $\Delta = 1 + b^2 r^2$ and $b = 2\pi N_t/L$ (N_t number of turns over the cylinder length L). Then,

$$\frac{B_\phi}{B_z} = \frac{r\partial\phi}{\partial z} = \frac{r2\pi N_t}{L} = br\alpha(r) = \frac{2b}{\Delta} \quad (5)$$

We assume a given value of the cylinder radius $r = R$, thus the line element results a function of the coordinate z : $s = s(z)$. The dependence with the radial component will be taken into account by considering different values of the radius R .

$$ds^2 = R^2 d\phi^2 + dz^2 = (1 + R^2 b^2) dz^2 = \Delta dz^2 \quad (6)$$

B. Thermal equilibrium

The thermal equilibrium is obtained, as in Paper I, assuming $L = 0$ in the balance energy equation (eq. 1). The procedure developed consists in obtaining the function of the temperature along the arc element s by integrating eq. 1 with the constraint $L = 0$ and replacing border conditions: the temperature at the bottom $T_b = 10^4 K$ and the temperature at the top $T_t = 10^6 K$. The known expression (see chapter 6 of Priest [15]) is obtained

$$\left[\frac{dT}{ds} \right]^2 = \frac{p^2 \chi}{2k_B^2 k_0 (\alpha + \frac{3}{2})} T^{\alpha - \frac{7}{2}} \left[1 - \left(\frac{T}{T_t} \right)^{2-\alpha} \right] \quad (7)$$

which has to be inverted to obtain $T = f^{-1}(s)$ [1] as

$$\frac{dT}{ds} = \mathcal{A} \left[\frac{d\mathbb{B}_v}{dv} \frac{dv}{dT} \right]^{-1} \quad \text{where} \quad \mathbb{B}_v \left(\frac{1}{2}, q \right) = \int_0^v t^{p-1} (1-t)^{q-1} dt \quad (8)$$

with

$$p = \frac{1}{2}; v = 1 - \left(\frac{T}{T_t}\right)^{2-\alpha}; q = \left(\frac{\alpha}{2} + \frac{3}{4}\right)(2 - \alpha) + 1$$

$$\mathcal{A} = (2 - \alpha)T_t^{\frac{\alpha}{2} - \frac{11}{4}} \left((p^2 \chi) / (2k_0(\alpha + \frac{3}{2})k_B^2) \right)^{\frac{1}{2}}.$$

We use $\alpha = -\frac{1}{2}$ so $q = \frac{6}{5}$ to numerically calculate the modes,

$$s = \frac{1}{\mathcal{A}} \mathbb{B}_v\left(\frac{1}{2}, \frac{6}{5}\right) \rightarrow \mathcal{A} = \frac{5}{2} T_t^3 \left(\frac{p^2 \chi}{2k_0 k_B^2} \right)^{1/2}.$$

Also, from boundary conditions $v = 0$, thus the constant value of the heating function results

$$H_0 = 7p^2 \chi T_t^{\alpha-2} / \left(8k_B^2 (\alpha + \frac{3}{2}) \right).$$

C. The perturbation

To calculate the stability and the structure of the modes the general perturbation along the equilibrium magnetic field is written

$$\vec{\xi} = [\zeta_r(r, z)\mathbf{e}_t + i\zeta_\phi(r, z)\mathbf{e}_\phi + \zeta_z(r, z)\mathbf{e}_z] e^{im\phi} \quad T_1 = T_1(r, z) e^{im\phi} \quad (9)$$

with $r = R$. The ϕ dependence only appears in the exponents that multiply the perturbation; the integration with respect to this coordinate is straightforward. Then, representing the equilibrium functions of the different quantities with a 0 sub-index, defining

$$\mathbf{e}_t = (Rb\mathbf{e}_\phi + \mathbf{e}_z) / \sqrt{\Delta} \quad \nabla_{\parallel} = \mathbf{e}_t (\mathbf{e}_t \cdot \nabla) \quad \rho_t = \frac{m_p}{k_B T_t}$$

with $\mathbf{e}_\phi, \mathbf{e}_z$ the cylindrical versors and \mathbf{e}_t the tangential versor, we obtain a non-dimensional expression for the energy principle of eq. 2:

$$\delta^2 W_p = \delta^2 W_c + \delta^2 W_m + \delta^2 W_{hc} + \delta^2 W_r \quad (10)$$

where $\delta^2 W_c$ is the generalized potential energy associated to compressional terms, $\delta^2 W_m$ corresponds to the magnetic contributions, $\delta^2 W_{hc}$ corresponds to the heat conduction terms and $\delta^2 W_r$ to the radiative contributions. The explicit form of these functions are given in the Appendix. The Bernstein's generalized potential energy corresponds to the magnetic contribution and part of the compressional one. In the generalized version of the energy principle additional terms appear in the $\delta^2 W_c$ term and also $\delta^2 W_{hc}$ and $\delta^2 W_r$ are entirely new terms.

IV. RESULTS AND DISCUSSION

Convective motion of the photosphere is believed to provide the energy that is storage in twisted magnetic coronal fields allowing the presence of long-lived coronal structures until it is released by instabilities ([16]; [23]). On the other hand, continuous spectra are generally associated to stability. An accepted conjecture establishes that unstable modes have a discrete spectrum (see [7] or [15]). There are two types of possible continuous spectra in this problem. The inhomogeneous character of the equilibrium parameters along the loop axis can lead to a continuum that couples to the Alfvén continuum [3]; e.g, when the disturbances considered are comparable to the inhomogeneous characteristic wavelength stable eigenvalues can give rise to a continuous spectrum ($L/2$, the equilibrium structure in the z component). This is the case studied in Paper I. On the other hand, GH established, for non vanishing helicity systems, that there is a continuous spectrum associated with the line-tied Alfvén resonance leading to the damping and heating by the resonant absorption mechanism and thus, directly relate to the stability of loops. They also pointed out how to obtain the resonant singular limit ω , from the class of physically permissible solutions,

$$\omega(r) = \frac{nB_z(r)}{\int_{-L}^L \sqrt{\rho(z)} dz}. \quad (11)$$

This resonance results because of the absence of an explicit dependence on the azimuthal magnetic field component (B_φ).

Thus, in order to understand in which conditions which mechanism can dominate and give account of the different scenarios i.e., the driving of the instability or the damping of mode oscillations, it is critical to gain knowledge about the dynamics and energetic contribution of twisted structures. Yet, the implications of the twisting in theoretical and observational descriptions are poorly known; e.g., there is no clarity about the modification of the dispersion relation and observational data are indirectly inferred.

In this paper we focused our attention to describe the changes in periods, stability and mode structure of coronal loops when the helicity, the magnetic field intensity and the radius are varied. For loops with vanishing helicity it is well established that the Alfvén line-tied resonance continuum is responsible of the damping of kink ($m = 1$) quasi-modes via the transfer of energy from the radial component into the azimuthal one, i.e., from discrete global modes into the local continuum modes where phase mixing can take place. Still,

the twisting of the magnetic field leads to the coupling of MHD cylindrical modes making difficult to provide a classification in terms of the behavior of pure-like modes.

In order to calculate modes and frequencies we followed the schematic procedure described in Paper I and in [8]. We used a symbolic manipulation program to integrate the equations. $\delta^2 W_p$ and the perturbations were expanded in a six dimensional-Fourier basis on the independent coordinate z that adjusts to border conditions, i.e., the four perturbed components (eq. 9) were expanded in a six mode basis to obtain 24 eigenvalues and eigenvectors for each of the helicity and the magnetic field values. Only the first eighteen eigenvalues were considered (the others are more than two order of magnitude smaller and accumulate at zero; the eigenvectors are also vanishingly small). Thus, a quadratic form for $\delta^2 W_p$ was obtained and was minimized with the Ritz variational procedure. A matrix discrete eigenvalue problem subject to a normalization constraint was obtained. From the resulting modes and the generalized potential energy (eq. 2): $\delta^2 W_p \geq 0$ the stability of each mode was determined.

The coronal loop parameters used were: $L = 10^{10}cm$ (or $L = 100Mm$), $T_b = 10^4K$, $T_t = 10^6K$, $n_e = 10^8cm^{-3}$ electron number density $p_t = 2k_B T_t$; $\rho_t = m_p p_t / k_B T_t$. Frequencies and modes were calculated for two different values of the magnetic field: $B_0 = 10G$ and $B_0 = 100G$, and for three different values of the helicity $b = (3.1 \cdot 10^{-8}; 3.1 \cdot 10^{-7}; 1.9 \cdot 10^{-6})$ which correspond to the adimensional values: $b_a = (2.8; 28; 170)$ with $N_t = (0.45; 4.3; 13.7)$, N_t : the number of turns over the cylinder length. These helicity values defined as weak, moderate and strong helicity respectively correspond to the classification given in [2] (Chapter 5). The adimensional radius was initially chosen as $R = 0.01$. In what follows we summarize the conclusions obtained from the data analysis which are displayed in three tables.

Table 1 shows the periods (in minutes) for weak, moderate and strong helicity for two values of the magnetic field intensity ($B_0 = 10G$ and $B_0 = 100G$ (left and right panel respectively)). S and U letters indicate the stable-unstable character of the modes. From the table we see that:

I) Weak helicity modes are stable. This is in accordance with the analytic results by Ruderman [19] who studied nonaxisymmetric oscillations of a thin twisted magnetic tube with fixed ends in a zero-beta plasma.

II) Higher modes have an accumulation point at zero, indicating the presence of a continuum spectra of stable modes (as in Paper I). Note that, calculus performed via discrete basis,

as in our case, give spectra that are necessarily discrete. Thus, an accumulation of discrete eigenvalues suggests a stable continuum spectrum.

III) The $B_0 = 10G$ case has larger periods than the $B_0 = 100G$ one. For moderate and strong helicity the eigenvalues of the first panel follow a scaling law with that of the second one i.e., they scale with the magnetic field intensity exactly as the Alfvén speed does $P_{10G} \simeq 10P_{100G}$.

IV) As HG and GH, we note a clustering of the spectra associated to the change from real to imaginary eigenvalues (and viceversa). There is a pronounced change (in the spacing of the periods or/and in the stability) from the sixth mode to the seventh mode. This is noted by a double line in Table 1 and related to the importance of the parallel component with respect to the perpendicular component (see Table 2). Up to period number ten real – imaginary eigenvalues of the first panel ($B_0 = 10G$) correspond to real–imaginary ones of the second panel ($B_0 = 100G$). Also, excepting large order periods $n > 10$, when the helicity is increased from weak to moderate the imaginary stable eigenvalues turn to imaginary unstable ones. For $B_0 = 10G$ and weak and moderate helicity cases there are five different groups of periods ($P_1 - P_6$; $P_7 - P_{10}$; $P_{11} - P_{12}$; $P_{13} - P_{14}$; $P_{15} - P_{18}$) (see also Table 2). The clustering is more difficult to establish i.e., the differences are less pronounced, with increasing magnetic field intensity and larger order periods.

In order to compare our results with those given by these authors we calculated the expression eq. 11 for our modes. We found that, all periods excepting $P_1 - P_6$ weak helicity modes satisfy the relation and thus, they belong to the Alfvén continuum spectrum justifying the scaling law described in III. As HG, we conclude that the change in the real–complex character of the $P_6 - P_7$ eigenvalues is associated to the existence of an accumulation point of the resonant Alfvén continuum, however we find that this change is not necessarily related to a change in the stability as they claimed. Note that all modes with weak helicity are stable (even the imaginary ones); in all the other cases the imaginary character of the eigenvalues is associated to instability. Yet, the continuum stable eigenvalue conjecture is here still valid [7], [15]; it applies to a spectrum with an accumulation point in zero; we found stable modes for all the helicity values and for the two magnetic field values with $P_{n>14}$. Note that the analysis of stable modes is still of interest because depending on the relative characteristic times of stable and unstable modes the stable ones could be active and accessible to observations.

The presence of at least one unstable mode means that the equilibrium state is unstable.

Thus, taking into account the whole range of stable modes, we confirm previous results leading to conclude that field configurations with some degree of twisting give a stabilizing effect allowing the storage of magnetic energy [17], i.e., when the helicity is augmented the stable weak case turns to an unstable one suggesting a critical value.

In Paper I, we obtained only one unstable mode classified as slow magnetoacoustic mode due to the almost longitudinal character (parallel to the magnetic field) of the wavevector perturbation and to the fact that the period did not change with the intensity of the magnetic field, resembling acoustic waves with sound speeds, v_s , independent of the magnetic field. The characteristic unstable time obtained in Paper I was $\tau_u = 36 \text{ min}$, corresponding to a typical slow magnetoacoustic fundamental period with a characteristic wavelength of the order of the loop length $L/2$. Also, we obtained a continuous set of stable modes classified as fast magnetoacoustic modes due to their large value component orthogonal to the magnetic field and to the fact that the eigenvalues scale with the intensity of the magnetic field as $P_{11G} \simeq 10P_{100G}$; thus resembling the dependence of the Alfvén waves $v_A \sim B_0$.

Table 2 (First Panel) displays the resulting features associated to the relative intensity of the parallel and perpendicular to the field components ($(\xi_{\parallel}, \xi_{\perp}, \xi_r)$ is an orthogonal basis) and their classification as slow-like (S) or fast-like (F). The relative phase between the components is also indicated in the table by P (in phase) and IP (inverted phase). Table 2 (Second Panel) also shows the intensity relationship between the cylindrical components. In order to classify the modes and to compare with the slow and fast magnetoacoustic modes obtained in Paper I, we calculated the cylindrical mode components and also the tangential and normal to the field components ($\xi_{\parallel} = (Rb\xi_{\phi} + \xi_z)/\Delta$; $\xi_{\perp} = (\xi_{\phi} - Rb\xi_z)/\Delta$). Our interest in the ξ_{\parallel} , ξ_z , ξ_r , ξ_{\perp} and ξ_{ϕ} components resides in that: First, when the helicity is weak, the ξ_{\parallel} component is expected to play the slow-mode role of ξ_z in Paper I. Second, the ξ_r component is related to the fast modes and determines the resonant absorption mechanism when uniform cylindrical flux tubes are considered by the transferring of energy to the ξ_{ϕ} component. When helicity and inhomogeneous distribution of equilibrium parameters are present it is worth investigating the transferring of energy from the ξ_r component to the others. In this case the resonant damping of global oscillations will occur by conversion of kinetic energy of the radial component into kinetic energy of the ξ_{\parallel} and ξ_{\perp} components; both components forming the plane orthogonal to ξ_r , and equal to the plane formed by ξ_{ϕ}

and ξ_z .

From the analysis of the amplitude of the components of the $P_1 - P_6$ modes with respect to the $P_7 - P_{18}$ ones in the weak helicity case i.e., real and imaginary eigenvector respectively, we could classify the first ones as slow-like modes because: I) their tangential components ξ_{\parallel} are at least an order of magnitude larger than the normal ones ξ_{\perp} ; II) as the helicity is weak $\xi_{\parallel} \approx \xi_z$ and $\xi_r \rightarrow 0$; $\xi_{\phi} \rightarrow 0$, the wavevector is almost tangential to the magnetic field; III) they have a larger characteristic time and a shorter characteristic speed than the imaginary eigenvectors. On the contrary, imaginary eigenvalues are associated to large values of the ξ_r component and ξ_{\perp} component (due to large values of ξ_{ϕ} (see Table 2 Second Panel)) , and small values of the ξ_{\parallel} and ξ_z components. As in Paper I, when the eigenvalues change from real to imaginary the period strongly diminishes and a change in the type of mode from the slow to fast magnetoacoustic type occurs. In opposition to Paper I where the acoustic mode has the same eigenvalue for both magnetic field intensities, here the modes are affected by the strengthening of the magnetic field leading to an-order-of-magnitude shorter period than in the non-helicity case. The ξ_{\parallel} and ξ_{\perp} components are in an inverted phase for real eigenvector modes and in phase for imaginary eigenvector modes.

For moderate helicity the overall description is similar but all the cases having non vanishing ξ_{ϕ} component and all the periods in the resonant line-tied continuum. As was mentioned, real-imaginary eigenvalues correspond to stable-unstable behavior.

In the strong helicity case, as the weak and moderate ones, we note for $P_1 - P_6$ larger, but comparable, values of the ξ_{\parallel} component with respect to the ξ_{\perp} component. In this case the two components of the mode are in phase. This relationship between the ξ_{\parallel} and ξ_{\perp} components of Table 2 (FP), and their associated phases is found again in the modes with $P_{15} - P_{18}$. In spite that these features are associated to the slow magnetoacoustic characterization, Table 2 (SP) shows that as ξ_z is vanishingly small, the strong helicity case cannot be classify as a slow mode.

When helicity is present the mixed character of the modes manifests itself making difficult to identify the components that are involved in the damping mechanism. However, taking into account the resonant frequency of eq. 11, we noted that (HG) all the modes, except those with $P_1 - P_6$ periods of the weak helicity case, have resonant frequencies suggesting that resonant absorption in helical modes is associated to modes with significant values of

ξ_{\perp} component. If this argument is correct we can affirm that the damping mechanism of body helical modes is associated to the transfer of kinetic energy of the radial component into kinetic energy of the ξ_{\perp} component which is not only related to the ξ_{ϕ} cylindrical contribution but also to the ξ_z one by the expression $\xi_{\perp} = (\xi_{\phi} - Rb\xi_z)\Delta$.

We also analyzed the change of the period as a function of the radius for different values of the helicity. We found that, for weak helicity, the increasing of the radius leads to a decrease of the periods. This is in accordance with observations, e.g., observed sausage modes are associated with thicker and denser loop structures and lower periods; while in other case (unstable cases) the increasing of the radius leads to an increase of the period.

Table 3 -First and Second Panel- shows the variation of the radius R with the twist bR for weak and moderate helicity respectively. [19] has conjectured that the line-tying condition at the tube ends should stabilize the tube and has suggested a critical value ($\sim Lb < q$; with q a positive constant and L the loop length) for the onset of instability. Also, [13] found that when the helicity grows beyond a critical value, the kink isolated twisted magnetic flux tubes below the photosphere become unstable. In fact, Table 3 can be seen as the variation of R with the twist value: bR , for constant values of the helicity b in the two cases: weak and moderate respectively. Stability is guaranteed when the loop radius is varied between $R = 0.01$ and $R = 0.1$ and the helicity is weak $b = 0.05$ (for almost the same value of the length of the loop, L). However, when the helicity is incremented to $b = 0.5$ even for the radius of $R = 0.01$ the loop structure is unstable, thus, instability can be associated with the presence of helicity values larger than a critical one.

Figure 1 shows the general potential energy for P_6 and P_7 in the weak and moderate cases. Note the change of this function when the system turns from stable to unstable, as helicity is augmented i.e., from $\delta^2 W_p > 0$ to $\delta^2 W_p < 0$. Figure 1a and Figure 1c display the total energy composed by the compressional, radiative, thermal and magnetic energy contributions of P_6 mode in the weak and moderate case respectively. The same features but for the P_7 mode are shown in Figure 1e and Figure 1g. Figure 1b and Figure 1d show the magnetic energy content alone for P_6 mode in the weak and moderate case respectively. Figure 1f and Figure 1h show the magnetic energy content for P_7 mode and for the weak and moderate case respectively. It can be seen, in this and in all the other cases, that the

magnetic energy content has a determinant role on the stability–instability of the system, i.e., the stability changes when the magnetic generalized potential energy changes sign. Thus, a result of this analysis is that the stability of twisted coronal loops is fundamentally determined by the storing of magnetic energy, being the other contributions less significant. Meanwhile, when the helicity is weak or vanishingly small and the magnetic contribution has a stabilizing effect the other non-dominant contributions, as the non-adiabatic ones, can play an important role. This makes possible, for example, the damping of fast excitations due to resonant absorption. Yet, even when one of these contributions is unstable, stable modes could be active for a while if their characteristic periods are shorter than the characteristic time of the instability. This is the case of Paper I, where we obtained a slow mode with an unstable characteristic times of $\tau \sim 36 \text{ min}$ coexisting with stable fast modes with periods about $P \sim 1 \text{ min}$; moreover, we showed that the instability can be nonlinearly saturated giving rise to a limit-cycle solutions, i.e., an oscillation between parallel plasma kinetic energy and plasma internal energy where the magnetic energy plays no relevant role. Thus, the contribution to the stable–unstable character of the modes is mostly due to the magnetic energy content and not to other energetic contributions. Note that as the balance energy equation takes into account non–adiabatic contributions, i.e., radiation, heat flow and heat function (with $L = 0$ at the equilibrium), the resulting perturbations are not constrained to the force–free condition. So, one result of the analysis is that the perturbation energy contribution is mainly due to magnetic forces. Thus, for these type of twisted magnetic field models, non–adiabatic perturbations (e.g. thermal perturbations) and resonant absorption seem unimportant to guarantee stability; a loop system with weak storage of magnetic energy (low values of the helicity) could be released if the helicity is suddenly increased, e.g., by footpoint motions. Meanwhile all the "zoo" of the coronal seismology can be active and accessible to observations.

V. APPENDIX: GENERALIZED POTENTIAL ENERGY TERMS

From the procedure described above and extensively exemplified in Paper I we can obtain -laboriously but in a straightforward way- the explicit terms for the energy principle given in eq. 10:

$$\delta^2 W_p = \delta^2 W_c + \delta^2 W_m + \delta^2 W_{hc} + \delta^2 W_r$$

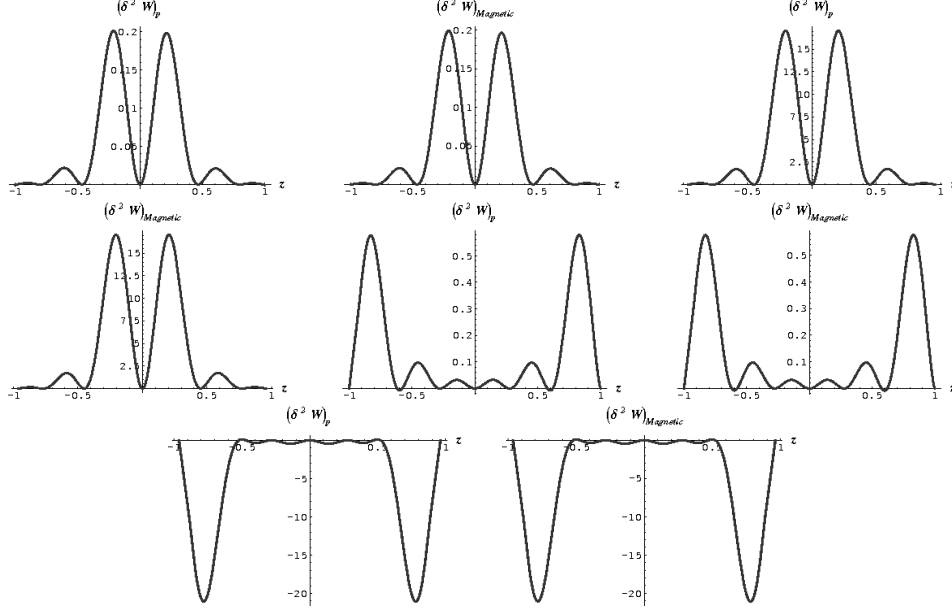


FIG. 1: Energy content of the sixth and seventh mode for $B_0 = 10G$. a) Total potential energy and b) magnetic potential energy respectively for the sixth mode $P_6 = 1.23 \text{ min}$ and for weak helicity. c) Total potential energy and d) magnetic potential energy respectively for the sixth mode $P_6 = 1.23 \text{ min}$ and for moderate helicity. e) Total potential energy and f) magnetic potential energy respectively for the seventh mode $P_7 = 0.07 \text{ min}$ and for weak helicity. g) Total potential energy and h) magnetic potential energy respectively for the sixth mode $P_7 = 0.07 \text{ min}$ and for moderate helicity.

where the right side of the equation corresponds to the compressional, magnetic, heat conduction and radiative contributions respectively. The compressional term $\delta^2 W_c = \delta^2 W_{c1} + \delta^2 W_{c2}$ has an additional contribution ($\delta^2 W_{c2}$) with respect to Bernsteins principle:

$$\delta^2 W_B = \delta^2 W_{c1} + \delta^2 W_m$$

$$\begin{aligned} \delta^2 W_{c1} = & \frac{1}{2} \int_{-1}^1 dz \beta \left\{ T_0 \rho_0 (1-m) \frac{\xi_r^2}{R^2} - \frac{m}{R} T_0 \left(\Delta \frac{d\rho_0}{ds} \xi_z \xi_\phi + \rho_0 \left(\frac{\xi_r \xi_\phi}{R} - \right. \right. \right. \\ & \left. \left. \left. - \frac{m}{R} \xi_\phi^2 + \frac{d\xi_\phi}{dz} \right) \right) + \Delta \frac{dT_0}{ds} \left(\Delta \frac{d\rho_0}{ds} \xi_z^2 + \rho_0 \left(\frac{\xi_r \xi_\phi}{R} - \frac{m}{R} \xi_\phi \xi_z + \xi_z \frac{d\xi_z}{dz} \right) \right) + \\ & + T_0 \left(\Delta^2 \frac{d^2 \rho_0}{ds^2} \xi_z^2 + \Delta \frac{d\rho_0}{ds} \xi_z \frac{d\xi_z}{dz} + \rho_0 \left(\frac{\xi_z d\xi_r}{R dz} - \frac{m}{R} \xi_z \frac{d\xi_\phi}{dz} + \xi_z \frac{d^2 \xi_z}{dz^2} \right) + \right. \end{aligned}$$

P_i	<i>weak</i>	<i>moderate</i>	<i>strong</i>	<i>weak</i>	<i>moderate</i>	<i>strong</i>
P_1	1.921 <i>S</i>	0.209 <i>S</i>	0.525 <i>i U</i>	0.159 <i>S</i>	0.021 <i>S</i>	0.052 <i>i U</i>
P_2	1.869 <i>S</i>	0.204 <i>S</i>	0.450 <i>S</i>	0.158 <i>S</i>	0.020 <i>S</i>	0.044 <i>S</i>
P_3	1.535 <i>S</i>	0.169 <i>S</i>	0.430 <i>S</i>	0.154 <i>S</i>	0.017 <i>S</i>	0.042 <i>S</i>
P_4	1.533 <i>S</i>	0.168 <i>S</i>	0.424 <i>i U</i>	0.153 <i>S</i>	0.0167 <i>S</i>	0.042 <i>i U</i>
P_5	1.306 <i>S</i>	0.143 <i>S</i>	0.206 <i>i U</i>	0.151 <i>S</i>	0.014 <i>S</i>	0.020 <i>i U</i>
P_6	1.228 <i>S</i>	0.135 <i>S</i>	0.177 <i>i U</i>	0.15 <i>S</i>	0.013 <i>S</i>	0.017 <i>i U</i>
P_7	0.068 <i>i S</i>	0.070 <i>i U</i>	0.125 <i>S</i>	0.0047 <i>i S</i>	0.007 <i>i U</i>	0.0125 <i>S</i>
P_8	0.064 <i>i S</i>	0.066 <i>i U</i>	0.122 <i>S</i>	0.0046 <i>i S</i>	0.006 <i>i U</i>	0.012 <i>S</i>
P_9	0.042 <i>i S</i>	0.044 <i>i U</i>	0.101 <i>S</i>	0.0044 <i>i S</i>	0.0043 <i>i U</i>	0.0101 <i>S</i>
P_{10}	0.041 <i>i S</i>	0.043 <i>i U</i>	0.100 <i>S</i>	0.0043 <i>i S</i>	0.0042 <i>i U</i>	0.01 <i>S</i>
P_{11}	0.033 <i>S</i>	0.036 <i>S</i>	0.989 <i>S</i>	0.0042 <i>i S</i>	0.0036 <i>S</i>	0.099 <i>S</i>
P_{12}	0.032 <i>S</i>	0.035 <i>S</i>	0.096 <i>S</i>	0.0041 <i>i S</i>	0.0035 <i>S</i>	0.0096 <i>S</i>
P_{13}	0.030 <i>i S</i>	0.031 <i>i U</i>	0.085 <i>S</i>	0.003 <i>S</i>	0.0031 <i>i U</i>	0.0086 <i>S</i>
P_{14}	0.027 <i>i S</i>	0.029 <i>i U</i>	0.081 <i>S</i>	0.0026 <i>S</i>	0.003 <i>i U</i>	0.0081 <i>S</i>
P_{15}	0.025 <i>S</i>	0.027 <i>S</i>	0.077 <i>S</i>	0.0025 <i>S</i>	0.0027 <i>S</i>	0.0077 <i>S</i>
P_{16}	0.024 <i>S</i>	0.026 <i>S</i>	0.076 <i>S</i>	0.002 <i>S</i>	0.003 <i>S</i>	0.0076 <i>S</i>
P_{17}	0.02 <i>S</i>	0.02 <i>S</i>	0.063 <i>S</i>	0.0024 <i>S</i>	0.0021 <i>S</i>	0.0063 <i>S</i>
P_{18}	0.018 <i>S</i>	0.02 <i>S</i>	0.059 <i>S</i>	0.0024 <i>S</i>	0.0025 <i>S</i>	0.006 <i>S</i>

TABLE I: Eighteen first periods associated to stable (S) and unstable (U) eigenvalues (minutes) for A) Left panel: $B_0 = 10G$ with A1) left column: weak helicity, A2) middle column: moderate helicity, A3) right column: strong helicity and B) Right panel: $B_0 = 100G$ with B1, B2, B3 the same as in A. Larger order modes were discarded.

$$\Delta \frac{d\rho_0}{ds} \left(\frac{\xi_r \xi_\phi}{R} - \frac{m}{R} \xi_\phi \xi_z + \xi_z \frac{d\xi_z}{dz} \right)$$

The magnetic contribution is:

$$\delta^2 W_m = C_1 \left\{ \beta \Delta \left(\frac{m}{R} B_\phi B_z \xi_r \xi_\phi - B_\phi B_z \frac{d\xi_r}{dz} \xi_z \right. \right. \\ \left. \left. - \left(\frac{B_\phi B_z}{R} + B_\phi \frac{dB_z}{dr} \right) \xi_r^2 + \left(\frac{m}{R} B_\phi B_z \xi_r \xi_\phi + B_\phi \frac{dB_\phi}{dr} \xi_r^2 \right) \right\} -$$

P_i	<i>weak</i>	<i>moderate</i>	<i>strong</i>	<i>weak</i>	<i>moderate</i>	<i>strong</i>					
P_1	$\xi_{\parallel} \gg \xi_{\perp} \mapsto 0$	S	IP	$\xi_{\parallel} > \xi_{\perp}$	S	IP	$\xi_{\parallel} \geq \xi_{\perp}$	P	$\xi_z \gg \xi_{\phi} \sim \xi_r \mapsto 0$	$\xi_z \gg \xi_{\phi} \sim \xi_r$	$\xi_r \leq \xi_{\phi}; \xi_z \mapsto 0$
P_2	$\xi_{\parallel} \gg \xi_{\perp} \mapsto 0$	S	IP	$\xi_{\parallel} > \xi_{\perp}$	S	IP	$\xi_{\parallel} \geq \xi_{\perp}$	P	$\xi_z \gg \xi_{\phi} \sim \xi_r \mapsto 0$	$\xi_z \gg \xi_{\phi} \sim \xi_r$	$\xi_r \leq \xi_{\phi}; \xi_z \mapsto 0$
P_3	$\xi_{\parallel} \gg \xi_{\perp} \mapsto 0$	S	IP	$\xi_{\parallel} > \xi_{\perp}$	S	IP	$\xi_{\parallel} \geq \xi_{\perp}$	P	$\xi_z \gg \xi_{\phi} \sim \xi_r \mapsto 0$	$\xi_z \gg \xi_{\phi} \sim \xi_r$	$\xi_r \leq \xi_{\phi}; \xi_z \mapsto 0$
P_4	$\xi_{\parallel} \gg \xi_{\perp} \mapsto 0$	S	IP	$\xi_{\parallel} > \xi_{\perp}$	S	IP	$\xi_{\parallel} \geq \xi_{\perp}$	P	$\xi_z \gg \xi_{\phi} \sim \xi_r \mapsto 0$	$\xi_z \gg \xi_{\phi} \sim \xi_r$	$\xi_r \leq \xi_{\phi}; \xi_z \mapsto 0$
P_5	$\xi_{\parallel} \gg \xi_{\perp} \mapsto 0$	S	IP	$\xi_{\parallel} > \xi_{\perp}$	S	IP	$\xi_{\parallel} \geq \xi_{\perp}$	P	$\xi_z \gg \xi_{\phi} \sim \xi_r \mapsto 0$	$\xi_z \gg \xi_{\phi} \sim \xi_r$	$\xi_r \leq \xi_{\phi}; \xi_z \mapsto 0$
P_6	$\xi_{\parallel} \gg \xi_{\perp} \mapsto 0$	S	IP	$\xi_{\parallel} > \xi_{\perp}$	S	IP	$\xi_{\parallel} \geq \xi_{\perp}$	P	$\xi_z \gg \xi_{\phi} \sim \xi_r \mapsto 0$	$\xi_z \gg \xi_{\phi} \sim \xi_r$	$\xi_r \leq \xi_{\phi}; \xi_z \mapsto 0$
P_7	$\xi_{\perp} \gg \xi_{\parallel} \mapsto 0$	F	P	$\xi_{\perp} > \xi_{\parallel}$	F	P	$\xi_{\perp} \geq \xi_{\parallel}$	IP	$\xi_r \sim \xi_{\phi} \gg \xi_z \mapsto 0$	$\xi_r \sim \xi_{\phi} \gg \xi_z \mapsto 0$	$\xi_z > \xi_r > \xi_{\phi}$
P_8	$\xi_{\perp} \gg \xi_{\parallel} \mapsto 0$	F	P	$\xi_{\perp} > \xi_{\parallel}$	F	P	$\xi_{\perp} \geq \xi_{\parallel}$	IP	$\xi_r \sim \xi_{\phi} \gg \xi_z \mapsto 0$	$\xi_r \sim \xi_{\phi} \gg \xi_z \mapsto 0$	$\xi_z > \xi_r > \xi_{\phi}$
P_9	$\xi_{\perp} \gg \xi_{\parallel} \mapsto 0$	F	P	$\xi_{\perp} > \xi_{\parallel}$	F	P	$\xi_{\perp} \geq \xi_{\parallel}$	IP	$\xi_r \sim \xi_{\phi} \gg \xi_z \mapsto 0$	$\xi_r \sim \xi_{\phi} \gg \xi_z \mapsto 0$	$\xi_z > \xi_r > \xi_{\phi}$
P_{10}	$\xi_{\perp} \gg \xi_{\parallel} \mapsto 0$	F	P	$\xi_{\perp} > \xi_{\parallel}$	F	P	$\xi_{\perp} \geq \xi_{\parallel}$	IP	$\xi_r \sim \xi_{\phi} \gg \xi_z \mapsto 0$	$\xi_r \sim \xi_{\phi} \gg \xi_z \mapsto 0$	$\xi_z > \xi_r > \xi_{\phi}$
P_{11}	$\xi_{\perp} \gg \xi_{\parallel} \mapsto 0$	F	P	$\xi_{\perp} > \xi_{\parallel}$	F	P	$\xi_{\perp} \geq \xi_{\parallel}$	IP	$\xi_r \sim \xi_{\phi} \gg \xi_z \mapsto 0$	$\xi_r \sim \xi_{\phi} \gg \xi_z \mapsto 0$	$\xi_z > \xi_r > \xi_{\phi}$
P_{12}	$\xi_{\perp} \gg \xi_{\parallel} \mapsto 0$	F	P	$\xi_{\perp} > \xi_{\parallel}$	F	P	$\xi_{\parallel} \geq \xi_{\perp}$	IP	$\xi_r \sim \xi_{\phi} \gg \xi_z \mapsto 0$	$\xi_r \sim \xi_{\phi} \gg \xi_z \mapsto 0$	$\xi_r > \xi_{\phi} > \xi_z$
P_{13}	$\xi_{\perp} \gg \xi_{\parallel} \mapsto 0$	F	P	$\xi_{\perp} > \xi_{\parallel}$	F	P	$\xi_{\perp} \geq \xi_{\parallel}$	IP	$\xi_r \sim \xi_{\phi} \gg \xi_z \mapsto 0$	$\xi_r \sim \xi_{\phi} \gg \xi_z \mapsto 0$	$\xi_z > \xi_r > \xi_{\phi}$
P_{14}	$\xi_{\perp} \gg \xi_{\parallel} \mapsto 0$	F	P	$\xi_{\perp} > \xi_{\parallel}$	F	P	$\xi_{\perp} \geq \xi_{\parallel}$	IP	$\xi_r \sim \xi_{\phi} \gg \xi_z \mapsto 0$	$\xi_r \sim \xi_{\phi} \gg \xi_z \mapsto 0$	$\xi_z > \xi_r > \xi_{\phi}$
P_{15}	$\xi_{\perp} \gg \xi_{\parallel} \mapsto 0$	F	P	$\xi_{\perp} > \xi_{\parallel}$	F	P	$\xi_{\parallel} \geq \xi_{\perp}$	P	$\xi_r \sim \xi_{\phi} \gg \xi_z \mapsto 0$	$\xi_r \sim \xi_{\phi} \gg \xi_z \mapsto 0$	$\xi_r > \xi_{\phi} > \xi_z$
P_{16}	$\xi_{\perp} \gg \xi_{\parallel} \mapsto 0$	F	P	$\xi_{\perp} > \xi_{\parallel}$	F	P	$\xi_{\parallel} \geq \xi_{\perp}$	P	$\xi_r \sim \xi_{\phi} \gg \xi_z \mapsto 0$	$\xi_r \sim \xi_{\phi} \gg \xi_z \mapsto 0$	$\xi_r > \xi_{\phi} > \xi_z$
P_{17}	$\xi_{\perp} \gg \xi_{\parallel} \mapsto 0$	F	P	$\xi_{\perp} > \xi_{\parallel}$	F	P	$\xi_{\parallel} \geq \xi_{\perp}$	P	$\xi_r \sim \xi_{\phi} \gg \xi_z \mapsto 0$	$\xi_r \sim \xi_{\phi} \gg \xi_z \mapsto 0$	$\xi_r > \xi_{\phi} > \xi_z$
P_{18}	$\xi_{\perp} \gg \xi_{\parallel} \mapsto 0$	F	P	$\xi_{\perp} > \xi_{\parallel}$	F	P	$\xi_{\parallel} \geq \xi_{\perp}$	P	$\xi_r \sim \xi_{\phi} \gg \xi_z \mapsto 0$	$\xi_r \sim \xi_{\phi} \gg \xi_z \mapsto 0$	$\xi_r > \xi_{\phi} > \xi_z$

TABLE II: First Panel: Intensity relationship between the tangential and normal to the field components of the eighteen first periods for $B_0 = 10G$ and for weak (first column), moderate (second column) and strong helicity (third column) cases. The (P) indicates in phase and (IP) indicates inverted phase. Second Panel: Intensity relationship between the cylindrical components of the eighteen first periods for $B_0 = 10G$ and for weak (first column), moderate (second column) and strong helicity (third column) cases.

$$\begin{aligned}
& -\beta \left((B_z^2 \frac{d\xi_r^2}{dz} + \frac{m^2}{R^2} B_{\phi}^2 \xi_r^2) + (B_{\phi}^2 \frac{d\xi_z^2}{dz} + 2B_{\phi} + \frac{dB_{\phi}}{dr} \xi_r \frac{d^2 \xi_z}{dz} + \frac{dB_{\phi}^2}{dr} \xi_r^2 + B_z^2 \frac{d^2 \xi_{\phi}}{dz}) + \right. \\
& \left. \left((B_z + R \frac{dB_z}{dr})^2 \frac{\xi_r^2}{R^2} - 2 \frac{m}{R^2} B_z (B_z + R \frac{dB_z}{dr}) \xi_r \xi_{\phi} + (\frac{m}{R} B_z)^2 \xi_{\phi}^2 + (\frac{m}{R} B_{\phi})^2 \xi_z^2 \right) \right) \Big\}
\end{aligned}$$

R	L	$R/2L$	$Twist = bR$	R	L	$R/2L$	$Twist = bR$
0.01	$9.05 \cdot 10^7$	0.005	0.028	0.01	$8.07 \cdot 10^7$	0.005	0.28
0.02	$9.04 \cdot 10^7$	0.01	0.057	0.015	$8.32 \cdot 10^7$	0.008	0.43
0.03	$9.02 \cdot 10^7$	0.015	0.085	0.02	$7.86 \cdot 10^7$	0.011	0.57
0.04	$8.99 \cdot 10^7$	0.02	0.11	0.025	$7.38 \cdot 10^7$	0.015	0.71
0.05	$8.96 \cdot 10^7$	0.025	0.14	0.03	$6.88 \cdot 10^7$	0.02	0.85
0.06	$8.9 \cdot 10^7$	0.03	0.17	0.04	$5.97 \cdot 10^7$	0.03	1.13
0.1	$8.7 \cdot 10^7$	0.05	0.28	0.05	$5.2 \cdot 10^7$	0.04	1.42

TABLE III: First Panel - Stable case: Variation of the Radius with the Twist for weak helicity $b = 0.05$ and $B_0 = 10G$. Second Panel - Unstable case: Variation of the Radius with the Twist for moderate helicity $b = 0.5$ and $B_0 = 10G$.

The heat conduction term results:

$$\delta^2 W_{hc} = -C_2 \left\{ 5 \frac{T_0^{3/2}}{\Delta} \frac{dT_0}{ds} T_1 \frac{dT_1}{dz} + T_1^2 \left(-T_0^{5/2} \left(\frac{mb}{\Delta} \right)^2 \frac{15}{4} T_0^{1/2} \frac{dT_0^2}{ds} + \frac{5}{2} T_0^{3/2} \frac{d^2 T_0}{ds^2} \right) + \frac{1}{\Delta^2} T_0^{5/2} T_1 \frac{d^2 T_1}{dz^2} \right\}$$

The new compressional contribution is expressed as:

$$\delta^2 W_{c2} = -\beta \left(\frac{m}{R} \rho_0 \xi_\phi T_1 + \Delta \frac{d\rho_0}{ds} \xi_z T_1 + \rho_0 \xi_z \frac{dT_1}{dz} \right)$$

and the term associated to radiation results:

$$\delta^2 W_r = -\alpha T_1^2 \rho_0^2 T_0^{\alpha-1} - \beta \left(\frac{m}{R} \rho_0 \xi_\phi T_1 + \Delta \frac{d\rho_0}{ds} \xi_z T_1 + \rho_0 T_1 \frac{d\xi_z}{dz} + \frac{\rho_0}{R} \xi_r T_1 \right)$$

where the following changes were made:

$$\rho \rightarrow \frac{\rho}{\rho_t}; \quad T \rightarrow \frac{T}{T_t}; \quad B_{\phi,z} \rightarrow \frac{B_{\phi,z}}{B_0}; \quad b \rightarrow bS$$

$$r, z \rightarrow \frac{r, z}{S}; \quad \delta^2 W_p \rightarrow \delta^2 W_p / (\chi T_t^{\alpha+1} \rho_t^2 L / m_p^2),$$

$S = \Delta L$ and the non-dimensional constants:

$$C_1 = \rho_t^2 T_t^{\alpha+1} B_0^2 / (\mu_0 k_B T_t n_e); \quad C_2 = c T_t^{\frac{7}{2}-\alpha} / (S^2 n_e^2).$$

were used. All the quantities were defined as in Paper I.

- [1] Arfken, G., Weber, H., 1995, "Mathematical methods for physicists" (San Diego:Academic Press).
- [2] Aschwanden, M. J. 2004, "Physics of the Solar Corona", (New York:Springer-Verlag).
- [3] Belien A.J.C., Poedt S., Goedbloed J.P. A&A, 1997, 322, 995
- [4] Bernstein I. B., 1958, PhRv, 109, 10
- [5] Costa A., González R., 2006, A&A, 458, 953
- [6] Costa A., González R., Sicardi Schifino A. C., 2004, A&A, 427, 353
- [7] Freidberg, J.P, 1982, Reviews of Modern Physics, 54, 3
- [8] Galindo Trejo J., 1987, SoPh, 108, 265
- [9] Goedbloed J. P., Halberstadt G., 1993, A&A, 280, 647
- [10] Goossens M., Andries J., Aschwanden M. J., 2002, A&A, 394, L39
- [11] Halberstadt G., Goedbloed J. P., 1994, A&A, 286, 275
- [12] Heyvaerts J., Priest E. R., 1983, A&A, 117, 220
- [13] Linton M. G., Longcope D. W., Fisher G.H., 1996, ApJ, 469, 954
- [14] Nakariakov V. M., Roberts B., Murawski K., 1997, SoPh, 175, 93
- [15] Priest E. R., 1982, "Solar Magneto-hydrodynamics" (Boston:Publishing Company)
- [16] Raadu M.A., Schmieder B., Mein N., Geesztelyi L., 1988, A&A, 197, 289
- [17] Raadu M.A., 1972, SoPh, 22, 425
- [18] Roberts B., 2000, SoPh, 193, 139
- [19] Ruderman M.S., 2007, SoPh, 246, 119
- [20] Sicardi Schifino A. C., Costa A., Ferro Fontán C., 1991, JMP, 32, 1350
- [21] Sturrock, P. A. 1994, "Plasma Physics, An Introduction to the Theory of Astrophysical, Geophysical and Laboratory Plasmas", (Cambridge University Press)
- [22] Van Doorselaere T., Andries J., Poedts S., Goossens M., 2004, ApJ, 606, 1223
- [23] Vrsnak B., Ruzdjak V., Rompolt B., 1991, SoPh, 136, 151